ATF2 phosphorylation is a key event in neuronal apoptosis, linking the DLK/LZK kinase cascade to JUN upregulation

Jorge Gomez-Deza[1], Matthew Nebiyou[1], Mor R. Alkaslasi[1], Lara H. El Touny[2], Anastasia L. Slavutsky [1], Nathan Ashby[1], Ken Cheng[2], Claire E. Le Pichon[1]

[1]*Eunice Kennedy Shriver* National Institute of Child Health and Human Development, National Institutes of Health, Bethesda, MD, USA

[2]Division of Preclinical Innovation, National Center for Advancing Translational Sciences, National Institutes of Health, Bethesda, MD, USA.

Abstract

Apoptotic neuron death is a common feature of many neurodegenerative diseases. Perhaps surprisingly, the exact mechanisms by which neurons undergo apoptosis have yet to be elucidated. We conducted an unbiased whole genome screen in human neurons to discover genes required for apoptotic neuron death, and discovered ATF2, MAP3K12 and JUN among top hits. We demonstrate that ATF2 is a previously unappreciated master regulator of neuron death. ATF2 is activated by phosphorylation downstream of dual leucine zipper kinase (DLK or MAP3K12) and leucine zipper kinase (LZK or MAP3K13) and its phosphorylation is essential for transcriptional upregulation of JUN. Contrary to previous assumptions, JUN phosphorylation is not required for apoptosis – just its upregulation. JUN phosphorylation is therefore simply a correlate of JUN upregulation. In this study, we identify phosphorylation of ATF2 as a key event in the mechanism of neuronal apoptosis, linking the DLK/LZK kinase cascade to transcriptional upregulation of JUN. Since targeting members of this signaling pathway to block neuronal death has proved difficult, ATF2 offers a novel and promising alternative.

Introduction

As post-mitotic cells lacking stem cells, most neurons cannot be replaced. Neuron death is a key hallmark of neurodegenerative conditions such as Alzheimer's disease (AD) and amyotrophic lateral sclerosis (ALS) or glaucoma, as well as a common consequence of brain injury and chemotherapeutic treatment. Neuron death can occur by different mechanisms including apoptosis, autophagy, ferroptosis, necrosis, and others[1]. Among these, apoptosis has been the most extensively studied form of cell death and is mediated by the caspase protein family. However, the precise mechanisms by which apoptosis occurs in neurons remain unclear. A better understanding of the molecular steps leading to neuron apoptosis could have significant value for patients suffering from diverse neurodegenerative conditions, from traumatic brain injury or chemotherapy-induced peripheral neuropathy to AD or ALS.

DLK is an evolutionarily conserved, neuronally enriched MAP triple kinase and a key regulator of axon degeneration and neuronal death. Leucine zipper kinase (LZK or MAP3K13) is a less well studied MAP triple kinase, despite sharing 90% homology of its kinase, catalytic, and leucine zipper domains with DLK[2]. Although much work has focused on understanding DLK, the importance of LZK in neuron degeneration and regeneration has only recently been appreciated[3–7]. Moreover, although DLK and LZK have been studied in mouse models, how these two proteins cooperate to regulate neuronal death in human neurons remains unknown. The DLK pathway has been recognized as a promising therapeutic target for many neurodegenerative conditions, prompting the development of DLK inhibitors[8–11]. However, a clinical trial testing DLK inhibitors in ALS patients was recently halted due to safety concerns[12], highlighting a pressing need to better understand the DLK/LZK pathway in human neurons and identify alternate candidate targets.

DLK regulates the neuronal transcriptional response to stress and injury via the phosphorylation of MAP2K4/7 and Jun N-terminal Kinase (JNK), which leads to the phosphorylation and activation of several transcription factors such as cJun[13]. cJun is regarded as a critical regulator of neurodegeneration by activating the transcription of pro-apoptotic factors. Whether cJun phosphorylation at serines 63 (S63) and 73 (S73) is necessary to drive apoptosis in neurons is still unclear[14–18]. This is one question we set out to address in this study.

cJun is a member of the activator protein-1 (AP-1) family of transcription factors, which is characterized by the presence of a basic leucine zipper (bZip) domain. Other AP-1 proteins include cFOS, ATF4, ATF3 and ATF2, which are known to form homo- and heterodimers to regulate transcription[19]. Activating transcription factors (ATF) are considered a subfamily of the AP-1 transcription factors. They share preferential binding to cAMP responsive elements (CRE) and include 7 members, ATF1-7[20]. Although ATF3 and ATF4 are relatively well characterized as contributors to neuronal injury responses[21–24], the role of ATF2 in neurons has been largely overlooked.

Studies in cell lines have revealed ATF2 can be phosphorylated by several proteins, including JNK, P38, and ERK[25], at threonines 69 and 71 (T69 and T71), inducing its translocation to the nucleus. Once in the nucleus it exerts its transcriptional activity by homo- and heterodimerizing with cJun and altering its nuclear distribution[26]. ATF2 is highly expressed in the brain and its depletion causes cranial motor neuron degeneration[27], highlighting its importance in neurodevelopment. While elevated ATF2 levels have been reported in AD[28,29] and Parkinson's

disease models[30], little is known about the mechanisms driving its translocation to the nucleus or its downstream targets in neurons.

To discover essential factors contributing to neuronal apoptosis, we performed whole-genome CRISPR interference (CRISPRi) screening on human neurons treated with vincristine. This chemotherapeutic agent is a microtubule destabilizer that disrupts the neuronal cytoskeleton and leads to apoptosis. Using this system, we identified dual leucine zipper kinase (DLK or MAP3K12), cJUN, and activating transcription factor 2 (ATF2), among others, as essential regulators of apoptosis in human neurons. We demonstrate that these factors function within a unified signaling cascade.

We show that DLK and LZK cooperate to induce neuron death by regulating the pro-apoptotic transcriptional response in human neurons. Each of these kinases is necessary for neuron death, which can only be prevented by blocking both. The phosphorylation of cJun is a reliable marker of DLK kinase pathway activation, which has led to an assumption that is likely necessary for neuron death downstream of DLK. However, we find that cJun phosphorylation is dispensable for vincristine-induced neurodegeneration, and rather that its transcriptional upregulation is key. Our experiments identify ATF2 phosphorylation as an essential driver of neurodegeneration that links DLK/LZK signaling to JUN transcription.

Results

Vincristine-induced neurodegeneration is transcription-dependent

To investigate the molecular mechanisms that lead to cell death in human neurons, we used a transcription factor-mediated platform to generate cortical (NGN2-driven[31]) and sensory (NGN2/BRN3A-driven[32]) neurons from iPSCs (Fig. 1A). We generated two human neuron subtypes to increase confidence in our results. Importantly, both types of neurons differentiated this way are transcriptionally similar to human neurons from postmortem tissue[32,33].

Us and others have shown that vincristine-induced axon degeneration is independent of transcription[34,35]. However, we wondered whether vincristine-induced neuronal death was dependent on transcription. Cell viability was assessed using an MTT assay in cortical and sensory neurons treated with 5 nM vincristine, in combination with two transcriptional inhibitors: Actinomycin D (ActD) and a cyclin dependent kinase 7 (CDK7) inhibitor, THZ1 2HCK (or CDK7i), for 48 hours. Vincristine treatment resulted in a significant reduction in neuron viability, which was rescued by inhibiting transcription using both ActD and CDK7i in both cortical and sensory human neurons (Fig. 1B and C). These results show that vincristine-induced neurodegeneration is transcriptionally driven.

DLK and LZK cooperate to regulate cell death in human neurons

DLK and LZK are highly homologous, neuronally enriched, stress-sensing proteins. They function by relaying cytoplasmic stress and initiating a transcriptional response that regulates the neuronal fate to injury. Much of the current literature has focused on understanding the role of DLK after stress or injury. Despite high homology in DLK's and LZK's functional domains, little is known about LZK's role after neuronal stress and its role in regulating transcription. DLK and LZK's kinase domains share a high degree of homology, making it impossible to use small molecule inhibitors to inhibit one protein without affecting the other. Therefore, we generated DLK, LZK, and DLK/LZK double mutants and differentiated them into cortical and sensory neurons to increase confidence in our results. Validation of DLK and LZK knockout was performed by PCR of the excised allele (Supp. Fig. 1A-D).

We asked whether DLK and LZK regulated cell death in human neurons in response to injury. To do so, we assessed the viability of wildtype (WT), DLK, LZK and DLK/LZK KO cortical and sensory neurons after 48 hours of vincristine treatment. WT, DLK and LZK KO, but not DLK/LZK KO cortical neurons showed a significant decrease in viability in response to vincristine exposure (Fig. 1D). We observed similar results in sensory neurons, where the deletion of both DLK and LZK fully protected neurons from degeneration, while DLK and LZK single KO was only partially protective (Fig. 1E).

Additionally, we measured the presence of phosphorylated H2AX (γH2AX), a marker of DNA damage that accumulates in the nucleus during cell death[36]. Treatment of vincristine for 24 hours resulted in a significant increase in the levels of γH2AX in WT neurons, which was significantly decreased in the DLK and LZK KO neurons, and completely abolished in the double DLK/LZK KO neurons (Fig. 1F and G). As a result, we conclude that DLK and LZK cooperate to regulate vincristine-induced neurodegeneration.

DLK and LZK regulate the transcriptional response to vincristine

Since we have shown that vincristine-induced neurodegeneration is transcription-dependent, and that DLK and LZK both regulate neuronal death, we set out to identify DLK, LZK and DLK/LZK-dependent transcriptional changes induced by vincristine. To do so WT, DLK, LZK and DLK/LZK KO neurons were treated with vincristine for 16 hours, and RNA sequencing (RNAseq) was performed. We chose this time point because inhibiting transcription up to 8 hours after vincristine addition prevented cell death (Supp Fig. 2A and B). We identified 154 differentially upregulated expressed genes in WT neurons after vincristine treatment (Fig. 2A and B). In contrast, only 9 and 11 genes were differentially upregulated in DLK and LZK KO neurons respectively, and the transcriptional response to vincristine was almost completely abolished in double DLK/LZK KO neurons (Fig. 1I and J). Gene ontology analysis of significantly upregulated genes revealed enrichment of genes involved in the regulation of apoptosis and regulation of endoplasmic reticulum stress in WT neurons in response to vincristine (Sup. Fig. 2C) and reduced in DLK, LZK and double DLK/LZK KO neurons (Sup. Fig 2D and E). Interestingly, DLK and LZK-dependent genes overlapped greatly (Fig. 1K), indicating that both proteins play overlapping roles in regulating transcription in human neurons.

DLK and LZK regulate total and phospho-cJun levels in human cortical neurons via JNK and transcription.

Phosphorylation of the transcription factor cJun (p-cJun) is widely regarded as a key regulator of DLK-dependent transcriptional responses [13]. We performed immunofluorescence on vincristine-treated WT, DLK, LZK and DLK/LZK KO neurons to measure the relative contribution of DLK and LZK to p-cJun levels. Interestingly, unlike mouse neurons where cJun phosphorylation is almost entirely dependent on DLK[37–39], we observed that in DLK and LZK KO neurons, the levels of p-cJun were significantly upregulated after vincristine, and only completely absent in double DLK/LZK KO neurons (Fig. 2A and B). We also measured the levels of total cJun in the nucleus. Similarly, the increase in total cJun levels after vincristine was only partially decreased DLK and LZK KO neurons, and completely absent in double KO neurons (Fig. 2C).

Our RNAseq results showed that JUN (which encodes cJun) levels were significantly upregulated in WT but not in double DLK/LZK KO neurons. To better understand how cJun and its phosphorylation are regulated, we treated WT neurons with vincristine in addition to GNE-3511 (a DLK/LZK inhibitor or DLKi), a Jun N-terminal Kinase (JNK) inhibitor (JNKi), and two transcription inhibitors (ActD and CDK7i). Treatment with all four inhibitors completely suppressed p-cJun increase after vincristine (Fig. 2D and E), indicating that the phosphorylation of cJun is not only regulated by the DLK/LZK-JNK pathway, but also by transcription. Additionally, total Jun levels were significantly decreased in neurons treated with all 4 inhibitors (Fig. 2F). This suggests that the observed increase in p-cJun levels may be due to a corresponding increase in total cJun levels. To test this, we performed double immunolabelling using an antibody recognizing p-cJun (S63) and a fluorescently conjugated antibody recognizing total cJun. Using this method, we were able to correlate the levels of both protein species in the nucleus of individual cells before and after

vincristine treatment. As expected, the levels of cJun and p-cJun (S63) highly correlated both before (black squares, Pearson correlation r=0.64 p<0.0001) and after (red triangles, Pearson correlation r=0.89 p<0.0001) vincristine treatment, indicating that both phospho- and total cJun increase simultaneously under stress (Fig. 2G).

Vincristine-induced neurotoxicity is driven by cJun but independently of its phosphorylation

We next wanted to investigate whether cJun regulates vincristine-induced cell death, and whether its phosphorylation at serines 63 and 73 is necessary for this process. To do so, I^3 iPSCs containing Zim3-dCas9[40] gene silencing machinery were transduced with control and JUN-targeting guide RNAs (gRNAs) which represses endogenous cJun expression. We performed a rescue experiment where control and JUN gRNA-expressing neurons were transduced with EGFP, WT cJun and cJun S63A S73A (cJun AA)-expressing lentivirus for 3 days and then treated with 5nM vincristine for 48 hours. Our results showed a robust decrease in cell viability in control gRNA neurons expressing EGFP, cJun and cJun AA when exposed to vincristine. On the other hand, JUN gRNA neurons expressing EGFP were protected from vincristine-induced neurodegeneration, but not those expressing both cJun and cJun AA (Fig. 2G). These results show that cJun is necessary for vincristine-induced neurodegeneration, but its phosphorylation at serines 63 and 73 is not. It also suggests that additional proteins may regulate the transcription of JUN to induce neuronal death.

Whole genome CRISPRi screen identifies JUN and ATF2 as upstream modifiers of neuronal apoptosis

To identify additional factors driving neurodegeneration in human neurons, we performed a whole genome CRISPR-interference (CRISPRi) screen. I^3iPSCs containing Zim3-dCas9 gene silencing machinery were transduced with a pooled library of dual sgRNAs targeting all genes in the genome, as well as 2500 non targeting controls. iPSCs that were infected with gRNAs were selected using puromycin and differentiated into mature cortical neurons for 10 days. Neurons were then treated with 10 nM vincristine for 48 hours, or DMSO as a control. Next generation sequencing was performed on the surviving neurons in both conditions to identify genes that promoted neuronal survival after vincristine treatment (Fig. 3A).

The CRISPRi screen was performed twice to increase reliability of our results using slightly different cell collection methods (Fig. 3B, see methods for details). Genes with a false discovery rate (FDR) of p<0.05 were considered as positive hits. Screen 1 and 2 identified 209 and 119 genes respectively, and the combination of both screen results revealed 46 common genes that protect neurons against vincristine-induced neurotoxicity (Fig. 3C). String analysis was performed to create a protein-protein interaction network of genes identified to reduce neuron degeneration (Fig. 3D). Further gene ontology analysis revealed these genes are involved ribosomal biogenesis, cytoplasmic translation as well as regulation of neuron apoptosis (Supp. Fig. 3A). However, we found that there was little overlap between the transcriptionally upregulated genes and genes found to be protective in our CRISPRi screen (Supp. Fig. 3B). Consistent with our previous results, JUN was identified as a driver of vincristine-induced neurodegeneration in human neurons (Fig.

3C, green). Interestingly, our results also identified a much lesser studied cJun interactor in neurons, the activating transcription factor-2 (ATF2) (Fig. 3C, red).

We validated our CRISPRi screen results by transducing Zim3-dCas9 iPSCs with gRNAs targeting JUN and ATF2 as well as a control gRNA and differentiated them into mature neurons. As expected, silencing of both JUN and ATF2 protected neurons from vincristine-induced neurotoxicity (Fig. 3E).

Neuronal injury induces p-ATF2 phosphorylation in a DLK/LZK dependent manner in vitro and in vivo

ATF2 and cJun are both AP1 transcription factors[26], known to form homo and heterodimers, enhancing each other's ability to regulate gene expression[26] (han embo). The nuclear import of ATF2 is regulated by phosphorylation[41]. We hypothesized that vincristine would increase the levels of phosphorylated nuclear ATF2 (p-ATF2) in a DLK and LZK dependent manner. As predicted, treatment of WT but not DLK, LZK or double DLK/LZK KO neurons with vincristine resulted in a significant increase in the levels of nuclear p-ATF2 (Fig. 4A and B). Treatment of neurons with DLKi and JNKi also abolished the increase of nuclear p-ATF2 after vincristine treatment (Fig. 4C). ATF2 phosphorylation can also be regulated by P38[25]. We observed no increase in the levels of phospho-P38 in neurons treated with vincristine (Supp. Fig. 4A and B) and inhibition of P38 did not significantly reduce vincristine-induced neuron death (Supp. Fig. 4C). Together our results show that DLK and LZK regulate ATF2 phosphorylation via the JNK pathway.

Moreover, we observed that nuclear p-ATF2 and cJun levels strongly correlated in response to vincristine exposure (red squares, Pearson correlation $r=0.79$, $p<0.0001$) and to a lesser extent in untreated neurons (black triangles, Pearson correlation $r=0.25$, $p<0.0001$) (Fig. 4D). We further validated that activation of the DLK/LZK pathways results in increased nuclear p-ATF2 levels by overexpressing GFP tagged DLK and LZK as well as two kinase dead mutants, DLK S302A and LZK K181A in HEK-239A cells. We found that expression of both WT DLK and LZK resulted in a significant increase in the nuclear p-ATF2 levels compared to kinase-dead controls (Fig. 4E and F).

Next, we asked whether regulation of p-ATF2 by DLK and LZK after neuronal injury is evolutionarily conserved. Optic nerve crush (ONC) has been shown to induce transcription-dependent neuronal death regulated by DLK[42]. Mice were treated with vehicle or GNE-3511 (DLKi), then subjected to an optic nerve crush and harvested one day post injury (1 DPI). We evaluated the presence of p-ATF2 in the nuclei of retinal ganglion cells (RGCs) by immunofluorescence. The levels of p-cJun are known to increase in a DLK/LZK dependent manner after ONC and were thus used as a control of injury and DLKi treatment. As expected, the p-cJun and total cJun levels were significantly increased in vehicle-treated ipsilateral RGCs but not in those of DLKi treated mice (Fig. 4H and I). Interestingly, we observed a robust increase of nuclear p-ATF2 levels in vehicle-treated mice, which was abolished upon DLKi treatment (Fig. 4G and J). Taken together, our results show that the phosphorylation of ATF2 in response to neuronal stress is driven by the DLK/LZK pathway both *in vivo* and *in vitro*.

ATF2 phosphorylation is necessary for neurodegeneration

Despite observing a robust increase in the levels in nuclear p-ATF2 after vincristine treatment, results from our RNA seq data showed that the levels of ATF2 RNA remained unchanged (Fig. 1H and supplementary table). Phosphorylation of ATF2 at threonine 69 and 71 (T69 and T71) have been associated with neurodegeneration[26]. We tested whether these two residues were necessary for vincristine-induced neuronal death. To do so, we performed a rescue experiment. Control, JUN and ATF2 gRNA neurons were transduced with EGFP, ATF2 and ATF2 T69A T71A (ATF2 AA)-expressing lentivirus for 3 days and then treated with 5nM vincristine for 48 hours. We observed no significant differences in the viability in the control neurons expressing all three constructs after vincristine treatment, suggesting that expression of ATF2 does not exacerbate neuron death. Moreover, knockdown of JUN protected neurons from vincristine-induced cell death despite expressing ATF2 and ATF2 AA suggesting that cJun lies downstream of ATF2. Finally, ATF2 gRNA-expressing neurons expressing WT but not ATF2 AA degenerated in response to vincristine treatment, indicating that the phosphorylation of ATF2 is necessary for vincristine-induced neurodegeneration (Fig. 4K).

ATF2 regulates cJun and p-cJun levels after vincristine treatment

ATF2 and cJun have been shown to form heterodimers which bind to AP-1 binding sites in the JUN promoter to regulate its transcription. We asked whether ATF2 regulates both total and phospho-cJun levels after vincristine treatment. Interestingly, vincristine treatment of control and JUN gRNA but not ATF2 gRNA-expressing neurons resulted in a significant increase in p-cJun (S63) levels (Fig. 5A and B). Total cJun levels were only increased in control but not cJun or ATF2 KD neurons (Fig. 4C). These results identify ATF2 as a key regulator of both total cJun protein levels and its phosphorylation.

ATF2 and cJun regulate a common set of genes in response to vincristine

To characterize whether ATF2 and cJun regulated a common set of genes, we performed RNAseq on Control, JUN and ATF2 gRNA-transduced neurons treated for 16 hours with 5nM vincristine. In untreated ATF2 and JUN gRNA neurons, ATF2 and JUN transcripts were significantly reduced respectively, validating our knockdown strategy (Supp. Fig. 5A and B). Consistent with the observed decrease in total cJun levels in untreated ATF2 gRNA neurons (Fig. 5C), JUN transcripts were also significantly downregulated in untreated ATF2 gRNA neurons (Supp. Fig. 5A) indicating that under homeostatic conditions, ATF2 regulates cJun protein levels by regulating its transcription.

As expected, control neurons underwent a robust transcriptional response and pro-apoptotic genes such as CASP3, BBC3 (which encodes for PUMA), JUN, BCL2L11 and HRK but not ATF2 were significantly upregulated, and their expression was attenuated in both JUN and ATF2 gRNA neurons (Fig. 5D). Genes regulated by both JUN and ATF2 overlapped almost completely (Fig. 5E). As a result, we conclude that both ATF2 and cJun regulate neuron degeneration as part as a common pathway.

Discussion

Here, we demonstrate that both DLK and LZK regulate neuronal death by modulating the phosphorylation of ATF2 *in vivo* and *in vitro*. Under conditions of neuronal stress, levels of phosphorylated ATF2 rise within the nucleus, promoting the transcription of JUN. We establish that, although cJun is essential for neuronal degeneration, this process is independent of its phosphorylation. Consequently, our findings unveil ATF2 as an evolutionarily conserved critical component of the DLK/LZK signaling pathway and a novel potential therapeutic target for neurodegenerative disorders in which the DLK pathway has been identified to play a role such as Alzheimer's[8,43] or disease or ALS[43,44].

While the DLK pathway has been extensively studied in mice, our knowledge of how DLK drives neurodegeneration in human neurons remains limited. To enhance the robustness of our results, we generated single DLK and LZK knockout (KO) and double DLK/LZK KO iPSCs, differentiating them into cortical and sensory neuronal subtypes. In mice, phosphorylation of cJun and neuronal death following NGF withdrawal and models of axonal injury are almost completely driven by DLK [39,42,45,46]. However, in human neurons, we discovered that these processes are partially driven by DLK and LZK individually, with both proteins cooperating and being necessary to induce neurodegeneration. We saw no differences in the levels of p-ATF2 induced by DLK and LZK overexpression in HEK-293A cells, suggesting that DLK and LZK are equally potent kinases. These results raise crucial questions regarding the differential regulation of neurodegeneration by DLK and LZK in mice and humans, warranting further investigation.

While DLK's role in transcription regulation has been previously established in various injury models[38,42], the significance of LZK had largely gone unnoticed until recently. Our work underscores LZK's equal importance as a stress sensing kinase. We show that DLK and LZK regulate a common set of genes. Aside from a few tubulin-encoding genes, the transcriptional response to vincristine is entirely dependent on both DLK and LZK. We therefore identify LZK as a master regulator of neurodegeneration in human neurons.

We were particularly surprised to observe that genes encoding for several tubulin genes were consistently downregulated independently of DLK/LZK, cJun and ATF2 after vincristine treatment. Since vincristine is a microtubule destabilizing agent[47], we hypothesize that the decrease may be driven by autoregulation and degradation of tubulin messenger RNA[48]. Little is known about the molecular mechanism of this process, and the details are only recently being uncovered with the discovery of TTC5[49,50], however the degradation of tubulin transcripts and its possible contribution to axon degeneration should be further investigated.

Additionally, we demonstrate that the phosphorylation of cJun in response to cytotoxic stress is dependent on transcription. We show that the increase in phospho-cJun levels is the result of the corresponding increase in total cJun RNA and protein. Upon close examination of the literature, we discovered that the standard practice in the field has been to report a stress-induced increase in cJun phosphorylation by normalizing phospho-cJun levels to the loading control, rather than total Jun protein levels. The question of whether the phosphorylation of cJun is necessary for

neurodegeneration remains highly debated[14–18,51]. and the opposing results may be due to the different models of neurodegeneration used. Our results indicate that in human neurons, cJun is actively transcribed and regardless of its phosphorylation status, drives neurodegeneration.

We focused on better understanding the role of ATF2 and its role as a driver of neurodegeneration. Studies performed in stable cell lines have shown that localization of ATF2 to the nucleus is dependent on its phosphorylation at residues T69 and T71[41]. However, the mechanism by which this happens in neurons remained unknown. Here we identify DLK and LZK as novel regulators of ATF2 phosphorylation *in vivo* and *in vitro*. It has been previously suggested that cJun and ATF2 belong to different branches of the DLK/LZK pathway, and that simultaneous silencing of both factors provides an enhanced neuroprotection[4]. We show that ATF2 regulates cJun transcription as well as total and phospho-cJun levels after stress, and that the levels of p-ATF2 and cJun strongly correlate in the nuclei of stressed neurons. Moreover, we show that ATF2 and cJun control a highly overlapping set of genes in response to cellular stress. We therefore conclude that ATF2 and cJun belong to a unified signaling pathway where ATF2 lies upstream of cJun, and downstream of DLK and LZK (Fig. 6).

Our work also opens the door to systematically identify the downstream targets of transcription factors in health and disease in human neurons. The generation of virtually pure human neuronal subtypes eliminates transcriptional contamination from other cell types and reduces the costs associated with addressing these questions. Other transcription factors, such as ATF4[23], CHOP[21], or CREB[52], have been implicated in neurodegeneration. Elucidating how these and other proteins signal, as well as exploring the overlap between them, will provide an invaluable tool for the neurodegenerative research community.

Here we present the first ever whole genome CRISPR interference (CRISPRi) screen to identify modifiers of vincristine-induced neurotoxicity in human neurons. We identify ATF2 an evolutionarily conserved component of the DLK/LZK pathway. Although silencing ATF2 itself may not prove therapeutically beneficial, targeting its pathological interactions with upstream and downstream effectors may be exploited as a potential therapeutic target. Its therefore important that crucial questions are addressed, such as how is ATF2 imported into the nucleus in human neurons? How do ATF2 and cJun interact? or whether the interaction of JNK and ATF2 can be blocked? This work also identifies multiple drivers of neurodegeneration that should be further explored by the field, and we highlight the feasibility of using small molecule cellular stressors to perform large scale survival screens to identify disease-relevant candidate genes

Methods

Immunofluorescence

Immunofluorescence was performed as previously described[35]. Briefly, 10-14 day old neurons were treated with the appropriate stressor and inhibitors and fixed with ice cold 4% PFA for 10 minutes at room temperature. Cells were washed once with PBS and permeabilized with 0.1% TritonX in PBS for 5 mins and blocked in 5% normal donkey serum (NDS) in PBS at room temperature for 1 hour. Cells were stained with the selected primary antibody overnight at 4 degrees in 2.5% Donkey serum. Cells were washed 3 times in PBS and stained with the appropriate secondary antibody at a concentration of 1:500 in 2.5% NDS for 1 hour at room temperature. Cells were washed three times with PBS and DAPI was used as a nuclear counterstain. Antibodies used: p-cJun (S63) (CST, cat. no. 9261S), total cJun (CST, cat. no. 9165) p-ATF2 (T71) (Abcam, cat. no. ab32019) 488-conjugated cJun (SCBT, cat. no.) p53 (CST, cat. no. 2524) p-P53 (S15) (CST, cat. no. 9284) pP38 (Y180, Y182) (CST, cat. no. 9211).

Western blotting

Western blotting was performed as previously described[35]. Briefly, cells were harvested in ice cold RIPA buffer (Invitrogen, cat. no. 89901) supplemented with protease inhibitors (Sigma, 11836153001) and PhosStop (Sigma, cat. no. 4906845001). Protein concentrations were calculated using a BCA assay (ThermoFisher, cat. no. 23225). 10-20 µg of total protein lysate was loaded into a 4–20% Mini-PROTEAN® TGX™ Precast Protein Gels (Biorad, cat. no. 4561095). Gels were transferred into PVDF membranes and blocked for 1 hour at room temperature in 5% BSA. Membranes were incubated with the primary antibody (primary antibodies, catalog numbers and concentrations listed below) in 2.5% BSA solution in a cold room, rocking, overnight. Membranes were washed 3 times with PBS 0.1% Tween solution. Secondary antibody (goat anti-rabbit HRP and IRDye® 680RD Goat anti-Mouse IgG) was incubated for 1 hour at room temperature at a concentration of 1:8000 in 2.5% BSA solution. Membranes were washed 3 times with PBS 0.1% Tween solution prior to developing. Western blots were developed using Clarity Western ECL Substrate (Biorad, cat. no. 1705061) or fluorescence and imaged using a ChemiDoc MP Imaging system (Biorad). Band intensity was quantified using FIJI imaging analysis software. Antibodies used: γH2AX (CST, cat. no. 9261S), DLK (Sigma cat. no. HPA039936), LZK (Sigma, cat. no. HPA016497), β Actin (Sigma, cat. no. A1978, 1:5000), GAPDH (CST, cat. no. 97166S).

Sensory neuron differentiation

Sensory neurons were differentiated as previously described[32]. Briefly, i^3 iPSCs were dissociated using Accutase (Life Technologies, cat. no. A1110501). Cells were plated in Matrigel-coated (1:100 Corning) plates in sensory neuronal induction media on day 0 (1:1 mix of Neurobasal (ThermoFisher cat. no. 21103049) and DMEM/F12 medium (ThermoFisher cat. no. 11320-033) supplemented with1× MEM nonessential amino acids (NEAA) (ThermoFisher, cat. no. 11140050), 10 µM ROCK inhibitor (Y-27632; Selleckchem, cat. no. S1049), 2 µg/ml doxycycline (Clontech, cat. no. 631311), 1X N2 supplement (Life Technologies, cat. no. 17502048), 1× B27 Plus Supplement

(ThermoFisher Scientific, cat. no. A3582801). Induction media was changed daily for 2 days. On day 3 of differentiation, cells were dissociated using Accutase and plated in dishes coated with Polyethyleneimine (Sigma, cat. no. 408727-100ML) and laminin (15ng/ml Corning, cat. no. 354232). Cells were plated in sensory neuronal maturation media (1:1 mix of Neurobasal (ThermoFisher cat. no. 21103049) and DMEM/F12 medium supplemented with1× MEM nonessential amino acids (NEAA) (ThermoFisher, cat. no. 11140050), 2 µg/ml doxycycline (Clontech, cat. no. 631311), 1X N2 supplement (Life Technologies, cat. no. 17502048), 1× B27 Plus Supplement (ThermoFisher Scientific, cat. no. A3582801), 10 ng/ml BDNF (PeproTech, cat. no. 450-02), 10 ng/ml NT-3 (PeproTech, cat. no. 450-03), 10 ng/ml GDNF (PeproTech, cat. no. 450-10 – 100 µg), 10 ng/ml NGF (R&D systems, cat. no. 256-GF-100), 1 mg/ml mouse laminin (Invitrogen, cat. no. 23017015). Half of the neuronal maturation media was removed and replenished with fresh media every 2-3 days.

Cortical neuron differentiation

I^3Neurons were differentiated as previously described[35]. Briefly, i^3 iPSCs were dissociated using Accutase (Life Technologies, cat. no. A1110501). Cells were plated in Matrigel-coated (1:100 Corning) plates in neuronal induction media on day 0 (Knockout Dulbecco's modified Eagle's medium (DMEM)/F12 medium; Life Technologies Corporation, cat. no. 12660012), 1X N2 supplement (Life Technologies, cat. no. 17502048), 1× GlutaMAX (ThermoFisher Scientific, cat. no. 35050061), 1× MEM nonessential amino acids (NEAA) (ThermoFisher Scientific, cat. no. 11140050), 10 µM ROCK inhibitor (Y-27632; Selleckchem, cat. no. S1049), and 2 µg/ml doxycycline (Clontech, cat. no. 631311). Neuronal induction media was changed once a day for 2 more days. On day 3 of induction, cells were dissociated using Accutase and plated in dishes coated with poly-L-ornithine (PLO; 0.1 mg/ml; Sigma, cat. no. P3655-10MG). Cells were plated in neuronal maturation media (BrainPhys medium (STEMCELL Technologies, cat. no. 05790), 1× B27 Plus Supplement (ThermoFisher Scientific, cat. no. A3582801), 10 ng/ml BDNF (PeproTech, cat. no. 450-02), 10 ng/ml NT-3 (PeproTech, cat. no. 450-03), 1 mg/ml mouse laminin (Invitrogen, cat. no. 23017015), and 2 µg/ml doxycycline). Half of the neuronal maturation media was removed and replenished with fresh media every 2-3 days

Generation of DLK and LZK KO iPSCs

DLK and LZK KO neurons were generated as previously described (cite me). WT cortical and sensory iPSCs were transfected with two gRNAs targeting exon 2 of the DLK gene gRNA1: CCCAGGCTCCCTGCTACTGCAT and gRNA2: TCCTTTGGCGTGGTGCTATGGG or LZK gene gRNA1: TTGAGAAGATCAAAAGTGAAGG and gRNA2: AGATGAAGAACTGATTCGAAGG and a Cas9-GFP expressing constructs. iPSCs were allowed to grow for two days, then colonies were dissociated to make single cells using Accutase for 10 minutes at 37°C and a serial dilution was performed in two 6-well plates in mTESR Plus Basal Media with ROCK inhibitor. iPSCs were allowed to grow until single colonies were visible, hand-picked using a P1000 pipette, and an individual colony was transferred to a well of a 24-well plate. Once confluent, 10% of the cells were used for passaging and DNA was extracted on the remaining 90% of the cells using a Qiagen DNA extraction kit (Qiagen; Cat. No. 69504). Clones were screened by PCR (DLK KO primers: Forward:

TCAGGTGAATGCTGAGCCAGC Reverse: TGGAGACTGTTGCTTCCCACACLZK KO primers: Forward: TCAGGGATTGAAACTCCTGGAA Reverse: GGGTGCCTGTTAACATCTGAAG). Cortical double DLK LZK KO cells were generated by additionally knocking down DLK in LZK KO iPSCs as described above. Sensory double DLK LZK KO cells were generated by additionally knocking down LZK in DLK KO iPSCs as described above. Single and double KO cortical and sensory neurons were further validated by western blotting.

CRISPRi library lentiviral packaging

The Human Genome-Wide CRISPRi Dual-sgRNA Library (Cellecta KIDHGW-105K-P, 5 CRISPRi dual-sgRNA construct/gene, subsequently referred to as KIDHGW) was packaged as follows: 80% confluent Lenti-X™ 293T cells (Takara Bio; #632180) were transfected in 15-cm plates using Lipofectamine 3000 transfection reagent (ThermoFisher; #L3000015) with 19.5 mg library plasmid, 13.3 mg psPAX2, 4.5 mg pMD2.G (Gift from Didier Trono; Addgene #12260 and 12259), 1.8 mg pAdvantage (Promega; #E1711) and 2.4 mL P3000 reagent diluted in 80 mL Opti-MEM I reduced serum medium (ThermoFisher #31985070); 60 mL Lipofectamine 3000 transfection reagent diluted into another 2.4 mL Opti-MEM and incubated at room temperature for 5 min. Diluted Lipofectamine 3000 was added to DNA mixture and incubated for another 5 min and added dropwise to plates. Sixteen hours later, medium was replaced with DMEM 10% FBS with 1x ViralBoost (Alstem; #VB100). Two days later, medium was collected, centrifuged and the supernatant was filtered through a 0.45um filter, mixed well with Lentivirus Precipitation Solution (Alstem; #VC100), incubated at 4°C overnight followed by centrifugation according to the manufacturer' protocol. Viral pellet was resuspended in Essential 8™ Flex Medium (ThermoFisher; #A2858501) in 1/40th of the collected media volume, aliquoted and stored at -80°C. Library titration was performed by infection of IPSCs $^{ZIM3\text{-}dCas9}$ with different virus dilutions followed by RFP assessment by flow cytometry on day 3 post infection.

Vincristine CRISPRi positive selection screen

IPSCs$^{ZIM3\text{-}dCas9}$ were dissociated by StemPro™ Accutase™ Cell Dissociation Reagent (ThermoFisher; #A1110501), counted and resuspended in Essential 8™ Flex Medium supplemented with 10 mM Y-27632 (Tocris; #1254) and 8 mg/ml polybrene (Thomas Scientific; #C788D57) and mixed with a volume of KIDHGW lentivirus corresponding to an 1600x representation with MOI of 0.3. Cells were then seeded on Matrigel-coated 15 cm dishes (20 million cells per 20 ml of Essential 8™ Flex Medium supplemented with 10 mM Y27632 and 8 mg/ml polybrene per 15 cm dish) overnight, followed by fresh medium replacement. One day later, medium was replaced with fresh Essential 8™ Flex Medium supplemented with 0.5 mg/mL puromycin (ThermoFisher; #A1113803) for 3 days. Selected cells were dissociated and seeded on new Matrigel-coated 15 cm dishes and taken through the 3 days pre-differentiation followed by seeding on poly-ornithine-coated dishes for cortical neuronal differentiation for 7-8 days (PMID: 29924488) while maintaining >1600x representation with 12 million cells per 15 cm dish in 42 plates.

Terminally differentiated cortical neurons $^{ZIM3\text{--}dCas9\ KIDHGW}$ were split into 2 groups: 1-treated with 10 nM vincristine (21 plates) or 2-DMSO vehicle (21 plates) for 48 hrs then dissociated following

a protocol adapted from Kirwan *et. al.* [53]. Briefly, cells were incubated with DNase I (Worthington Biochemical Corporation) for 10 min at 37 °C, then washed in PBS and dissociated using TrypLE (ThermoFisher; # 12604021) with 5 units/ml papain (Worthington; # LK003178) and 1mM EDTA, resuspended in BrainPhys™ Neuronal Medium (Stem Cell Technologies; #05790) supplemented with DNAse I (1000 units/30 ml) (Worthington; # LK003172), 10 mM Y-27632 and 0.5 mM EDTA, pelleted, washed, re-pelleted and snap frozen. Genomic DNA was harvested with NucleoSpin Blood XL, Maxi kit for DNA from blood (Macherey-Nagel) or QIAamp® DNA Mini (Qiagen) including proteinase K digestion, for control and vincristine-treated groups, respectively. The screen was repeated twice. DNA was amplified and sequenced by Cellecta with >500 reads/sgRNA according to their NGS prep kit (#LNGS-400) and sequenced on a NextSeq 500 (Illumina). Counts files of DMSO and vincristine -treated samples subject to comparison were input into MAGeCK-including Negative Controls (https://kampmannlab.ucsf.edu/mageck-inc) where $\log_2$ fold changes (LFCs) and p values were calculated for each sgRNA using the 'mageck test –k' command, followed by Robust Rank Aggregation (RRA). RRA fits a negative binomial model to test whether the initial sgRNA counts (DMSO) vary significantly from the final condition's counts (Vincristine treatment)[54]. The resulting guide-level p values are combined at the gene level using a modified robust ranking algorithm, with corresponding estimated false discovery rates (FDRs) in the gain-of-function screen (vincristine resistance).

MTT assay

After differentiation, 50,000 cells per well were plated in 96 well plates (cat number) and differentiated for 10-14 days. Cells were treated with the appropriate stressor in 100 µl of neuronal medium. After treatment, MTT assay (Sigma, cat. no. CT02) was performed following the manufacturer's recommendations. Briefly, 10 µL of solution A was added to each well and placed in the incubator for 4 hours. 100 µL of solution B was added to each well and placed in the incubator overnight. Cell viability was measured using a microplate reader at 570nm. Chemical inhibitors and concentrations used: Actinomycin D (ActD) (Selleckem, cat. no. S8964; 3µM), THZ1 2HCK (CDK7i) (Selleckem, cat. no. S7549; 10 nM), DLKi (GNE-3511) (Cayman Chemical, cat. no. 19174; 500nM), Vincristine (Sigma, cat. no. V8879-5MG), P38 inhibitor (SB202190) (Tocris, cat. no.1264; 100nM).

RNA extraction for RNA seq

For RNA extraction, 2.5 million neurons were pleated in 6 well plates (Thomas scientific, cat. no. 1198D71) and differentiated for 10-14 days. Neurons were treated with DMSO or 5nM vincristine for 16 hours before RNA extraction. Neurons were washed once with PBS and harvested in 700 µL Qiazol (Qiagen, cat. no. 79306) and immediately placed on ice. RNA extraction was performed using RNeasy Mini Kit (Qiagen, cat. no. 74104) following the manufacturer's instructions. Columns were treated with RNase-Free DNase (Qiagen, cat. no. 79254), and RNA was eluted in 25 µL of RNAse free water. Eluted RNA was separated into two tubes, one containing 2 µL, subsequently used for quality control and another one containing the rest of the RNA used for RNA seq.

For RNA sequencing, 1-4 µg of total RNA samples were purified with PolyA extraction, and then purified mRNAs were constructed to RNA-Seq libraries with specific barcodes using illumina TruSeq Stranded mRNA Library Prep Kit. All the RNA-Seq libraries were pooled together and sequenced using illumina NovaSeq 6000 to generate approximately ~40 million 2x100 paired-end reads for each sample. The raw data were demultiplexed and analyzed further.

RNA seq analysis

Sequenced reads from all genotypes were trimmed to remove adaptor sequences using cutadapt v3.4 with the following parameters: -a AGATCGGAAGAGCACACGTCTGAACTCCAGTCA -A AGATCGGAAGAGCGTCGTGTAGGGAAAGAGTGT -q 20 --minimum-length 25. Trimmed reads were aligned to GRCh38 human reference GENCODE release 28 using STAR 1-pass v2.7.8.a[55] with the following parameters: --outFilterType BySJout --outFilterMultimapNmax 20 --alignSJoverhangMin 8 --alignSJDBoverhangMin 1 --outFilterMismatchNmax 999 --outFilterMismatchNoverReadLmax 0.04 --alignIntronMin 20 --alignIntronMax 1000000 --alignMatesGapMax 1000000 --outSAMtype BAM SortedByCoordinate. Quantitation of aligned reads was performed using the featureCounts of the subread package v2.0.1[56] with annotation sourced from GRCh38 human reference GENCODE release 28 and the following parameters: -s2 -p. After removing outliers, loss-of-function of DLK and LZK genes was analyzed using four Vinc-treated and four untreated biological replicates across the WT, DLK KO, LZK KO, and DLK/LZL double-KO cortical neurons. Loss-of-function of Jun and Atf2 genes was analyzed using five Vinc-treated and five untreated biological replicates in both Control and JUN KO cortical neurons, as well as four Vinc-treated and five untreated ATF2 KO cortical neurons. Differentially expressed genes (DEGs) were analyzed by comparing Vinc-treated cells to untreated cells based on the design '~treatment + 0' using DESeq2 v1.30.1 in R v4.0.3 (https://cran.r-project.org). Log2-transformed fold changes were computed using the 'ashr' shrinkage method[57] implemented in DESeq2. Genes were considered statistically significant if the false discovery rate (FDR) was below 0.1. The FDR was calculated using Benjamini-Hochberg (BH) method[58]. MA plots were created by plotting the mean normalized read counts on the x-axis and log2 fold changes on the y-axis across genes using ggplot2 in R.

Lentivirus production

Lentivirus were generated as previously described[35]. In one 10cm dish, 7 million Lenti-X HEK-293T cells (Takara Bio, cat. no. 632180) were seeded in 9 mL DMEM (Gibco, cat. no 11995065) supplemented with 10% FBS (Gibco, cat. no. 10437028). The next day, a transfection mix was prepared containing 1 µg of Lenti plasmid, 3 µg of third generation packaging mix (1:1:1 mix of three plasmids), 12 µL Lipofectamine 3000 Reagent (ThermoFisher, cat. no. L3000008), and XXX µL Opti-MEM I Reduced Serum Medium (GIBCO, cat. no. 31985070). The mix was vortexed, spun down briefly, incubated at room temperature for 40 minutes, then added dropwise to the HEK cells and gently swirled to mix. The next day, the media was replaced with 18 ml fresh 10% FBS DMEM supplemented with 1:500 ViralBoost (Alstem, Cat. No. VB100). After two days of incubation, the media was collected into a 50 ml Falcon tube, supplemented with 6 ml Lenti-X Concentrator (Takara Bio; Cat. No. 631231), mixed thoroughly, and stored at 4°C for 48 hours. The

supernatant was then spun down at 4°C for 45 minutes at 1,500 x g. The supernatant was aspirated, and the pellet was resuspended in 300 μL of PBS.

Statistical analysis

All quantification of microscopy images was performed blinded. Statistical analyses were performed using GraphPad Prism 9. Gene ontology analysis was performed in R version 4.0.3 (2020-10-10). String analysis was performed with https://string-db.org version 11.5. Venn diagrams were generated using Venny 2.1 (https://bioinfogp.cnb.csic.es/tools/venny).

Optic nerve crush

Mice were anesthetized with isoflurane, and artificial tears ointment was applied on the non-surgical eye. Crush injury was delivered to the left eye using an intra-orbital approach. The conjunctival layers were incised with a pair of fine scissors and two pairs of #5 fine forceps were used to gently separate the soft tissue in the intra-orbital space behind the eye until the optic nerve was visible. A pair of #5 forceps was used to manually crush the optic nerve for 5 seconds. The eyeball was gently pushed back into the orbit, and analgesia (6 mg/kg Meloxicam) was delivered subcutaneously. Animals were then returned to their home cages and monitored.

Tissue collection and processing.
Animals were injected intraperitoneally with 2.5% Avertin and decapitated. The eyes were removed from the skull and the proximal optic nerve was collected and rapidly frozen on dry ice. The eyes were fixed in 4% paraformaldehyde for 1 hour, and then stored in 1X PBS. Prior to sectioning, the eye was cryopreserved in 30% sucrose. The cornea was removed and the eye cup, including the retina, was frozen in OCT for cryosectioning at 16 µm onto positively charged slides using a Leica CM3050 S Research Cryostat.

Immunohistochemistry

Sections were thawed at 9room temperature for 10 minutes and washed twice with PBS and twice with 0.1% TritonX in PBS (0.1% PBST) for 10 minutes. Sections were blocked for 1 hour at room temperature with 5% normal donkey serum (NDS) in 0.1% PBST. Sections were stained with the selected primary antibody overnight at 4 degrees in 0.5% Donkey serum in 0.1% PBST. Primary antibody was washed four times with 0.1% PBST for 10 minutes at room temperature. Secondary incubation was performed by using the appropriate secondary antibody at a concentration of 1:500 in 0.1% PBST for one hour. Secondary antibody was washed four times with 0.1% PBST for 10 minutes at room temperature. Neurotrace (ThermoFisher, Cat. No. N21483) labelling was performed by diluting at a concertation of 1:600 in PBS and incubating for 30 minutes. Sections were washed three times with PBS and DAPI was used as a nuclear counterstain. Antibodies used: p-cJun (S63) (CST, cat. no. 9261S), total Jun (CST, cat. no. 9165) p-ATF2 (T71) (Abcam, cat. no. ab32019).

HEK cell culture and transfection

HEK-293A cells were cultured in DMEM (Gibco, cat. no 11995065) supplemented with 10% FBS (Gibco; cat. no. 10437028). For transfection, cells were dissociated using Trypsin-EDTA (0.25%) (ThermoFisher, Cat. No. 25200056) and plated in DMEM, 10%FBS. The day after plating cells were transfected with 1 µg DNA plasmid, 8 µl lipofectamine 2000 (Invitrogen, Cat. No. 11668030) for 24 hours. Cells were fixed with 4% cold PFA for 10 minutes, washed once with PBS and immunocytochemistry was performed.

Animal protocol

All animal care and experimental procedures were performed in accordance with animal study proposals approved by the National Institute of Child Health and Human Disease Animal Care and Use Committee (animal protocol number 20-003, Le Pichon lab). C57Bl/6J (Jax#000664) mice of both sexes, aged between 6-10 weeks old, were used in this study.

Figure legends

Figure 1:

A) Schematic representation of cortical and sensory i^3Neuron differentiation.
B) Quantification of the relative viability of cortical i^3Neurons after 48 hours of 5 nM vincristine, 5 nM vincristine + 30 nM ActD or 5 nM vincristine + 10 nM CDK7i treatment. N=3 independent differentiations. One-way ANOVA, Bonferroni correction (ns = not significant, p<0.005 ***, p<0.001 ****).
C) Quantification of the relative viability of sensory i^3Neurons after 48 hours of 5 nM vincristine, 5 nM vincristine + 30 nM ActD or 5 nM vincristine + 10 nM CDK7i treatment. N=3 independent differentiations. One-way ANOVA, Bonferroni correction (ns = not significant, p<0.005 ***, p<0.001 ****).
D) Representative western blots of WT, DLK, LZK and double DLK/LZK KO cortical i^3Neurons untreated (UT) and treated with 5 nM vincristine for 24 hours. Immunoblot for γH2AX and loading control GAPDH.
E) Quantification of relative γH2AX levels after 5 nM vincristine for 24 hours in WT, DLK, LZK and double DLK/LZK KO cortical i^3Neurons. Results normalized to UT. Results are represented as mean ± SEM. N=4 independent differentiations. Two-way ANOVA, Bonferroni correction. (p<0.005 ***, p<0.001 ****).
F) Quantification of the relative viability of WT, DLK, LZK and double DLK/LZK KO cortical i^3Neurons after 48 hours of 5 nM vincristine. N=4 independent differentiations. Two-way ANOVA, Bonferroni correction (ns = not significant, p<0.05 *, p<0.01 **, p<0.001 ****).
G) Quantification of the relative viability of WT, DLK, LZK and double DLK/LZK KO sensory i^3Neurons after 48 hours of 5 nM vincristine. N=3 independent differentiations. Two-way ANOVA, Bonferroni correction (ns = not significant, p<0.05 *, p<0.01 **, p<0.001 ****).
H) MA plots showing the transcriptional changes in WT, DLK, LZK and double DLK/LZK KO cortical i^3Neurons 16 hours after 5nM vincristine treatment. Genes that are significantly differentially expressed are labelled in red.
I) Number of differentially expressed genes in WT, DLK, LZK and double DLK/LZK KO cortical i^3Neurons 16 hours after 5nM vincristine treatment.
J) Venn diagram showing the common genes regulated by DLK and LZK after vincristine treatment.

Figure 2:

A) Representative images of WT, DLK, LZK and double DLK/LZK KO cortical i^3Neurons 24 hours after 5nM vincristine treatment. Immunostaining for p-cJun (S63) (green), DAPI (blue). (Scale bar = 15 µm).
B) Quantification of relative nuclear p-cJun (S63) levels UT and after 5 nM vincristine for 24 hours in WT, DLK, LZK and double DLK/LZK KO cortical i^3Neurons. Results normalized to WT UT. Results are represented as mean ± SEM. N=3 independent differentiations. Two-way ANOVA, Bonferroni correction. ($p<0.05$ *, $p<0.01$ **, $p<0.005$ ***, $p<0.001$ ****).
C) Quantification of relative nuclear total cJun levels UT and after 5 nM vincristine for 24 hours in WT, DLK, LZK and double DLK/LZK KO cortical i^3Neurons. Results normalized to WT UT. Results are represented as mean ± SEM. N=3 independent differentiations. Two-way ANOVA, Bonferroni correction. ($p<0.01$ **, $p<0.005$ ***).
D) Representative images cortical i^3Neurons 24 hours after 5nM vincristine, 5nM vincristine + DLKi (GNE=3511, 500nM), + JNKi (1 nM), ActD (30nM), CDK7i (10nM) treatment. Immunostaining for p-cJun (S63) (green), DAPI (blue). (Scale bar = 15 µm).
E) Quantification of relative nuclear p-cJun (S63) levels in cortical i^3Neurons 24 hours after 5nM vincristine, 5nM vincristine + DLKi (GNE-3511, 500nM), + JNKi (1 nM), ActD (30nM), CDK7i (10nM) treatment. Results normalized to UT. Results are represented as mean ± SEM. N=3 independent differentiations. One-way ANOVA, Bonferroni correction. (ns = not significant, $p<0.05$ *).
F) Quantification of relative nuclear cJun levels in cortical i^3Neurons 24 hours after 5nM vincristine, 5 nM vincristine + DLKi (GNE-3511, 500nM), + JNKi (1 nM), ActD (30nM), CDK7i (10 nM) treatment. Results normalized to UT. Results are represented as mean ± SEM. N=3 independent differentiations. One-way ANOVA, Bonferroni correction. ($p<0.005$ ***).
G) Correlation and Pearson r correlation coefficient of the nuclear levels of p-cJun (S63) and total cJun levels in UT (Black) and 5 nM Vincristine (red) cortical i^3Neurons for 24 hours.
H) Quantification of the relative viability of Control and JUN gRNA cortical i^3Neurons Untreated (UT) and transduced with EGFP, cJun and cJun S63A S73A (JunAA) after 48 hours of 5 nM vincristine. N=3 independent differentiations. Two-way ANOVA, Bonferroni correction (ns = not significant, $p<0.005$ ***).

Figure 3:

A) Schematic representation of the whole genome CRISPRi survival screen to identify modifiers of neuronal apoptosis in human neurons.
B) Top genes identified to promote neuron survival in screens 1 and 2. A smaller RRA score indicates a stronger survival effect.
C) Venn diagram showing the common genes identified to significantly prevent vincristine-induced neuronal apoptosis in two whole genome CRISPRi survival screens. False discover rate (FDR) ≤ 0.05.
D) Protein-protein interaction network for proteins identified to suppress vincristine-induced neuronal apoptosis in three whole genome CRISPRi survival screens. ATF2 and JUN are highlighted in red and green respectively.
E) Quantification of the relative viability of Control, JUN gRNA and ATF2 gRNA cortical i^3Neurons after 48 hours of 5 nM vincristine. N=3 independent differentiations. Two-way ANOVA, Bonferroni correction (ns = not significant, $p<0.005$ ***).

Figure 4:

A) Representative images of WT, DLK, LZK and double DLK/LZK KO cortical i^3Neurons UT and 24 hours after 5nM vincristine treatment. Immunostaining for p-ATF2 (T71) (green), DAPI (blue). (Scale bar = 20 µm).
B) Quantification of relative nuclear p-ATF2 (T71) levels UT and after 5 nM vincristine for 24 hours in WT, DLK, LZK and double DLK/LZK KO cortical i^3Neurons. Results normalized to WT UT. Results are represented as mean ± SEM. N=3 independent differentiations. Two-way ANOVA, Bonferroni correction. (ns = not significant, $p<0.01$ **).
C) Quantification of relative nuclear p-ATF2 (T71) levels UT and after 5 nM vincristine and 5nM vincristine + DLKi (GNE=3511, 500nM), + JNKi (1 nM) for 24 hours in cortical i^3Neurons Results normalized to UT. Results are represented as mean ± SEM. N=3 independent differentiations. One-way ANOVA, Bonferroni correction. (ns = not significant, $p<0.05$ *).
D) Correlation and Pearson r correlation coefficient of the nuclear levels of p-ATF2 and total cJun levels in UT (Black) and 5nM Vincristine (Red) cortical i^3Neurons for 24 hours.
E) Representative images of HEK-239A cells transfected with DLK-GFP, DLK-S302A-GFP, LZK-GFP and LZK-K181A-GFP for and immunostaining for p-ATF2 (T71) (red), DAPI (blue). (Scale bar = 20 µm).
F) Quantification of relative nuclear p-ATF2 (T71) levels in HEK-239A cells transfected with DLK-GFP, DLK-S302A-GFP, LZK-GFP and LZK-K181A-GFP for 24 hours. One-way ANOVA, Bonferroni correction. (ns = not significant, $p<0.05$ *, $p<0.01$ **).
G) Representative images of retinas uninjured and 1 day post injury (1DPI) in mice treated with vehicle (Veh.) or DLK inhibitor GNE-3511 (DLKi). Immunostained with p-ATF2 (T71) (red), neurotrace (yellow) and DAPI (blue).
H) Quantification of relative nuclear p-cJun (S63) levels in the nucleus of retinal ganglion cells in mice treated with vehicle (Veh.) or DLK inhibitor GNE-3511 (DLKi) contralateral (con) and ipsilateral (ipsi) 1 day after optic nerve crush. N=3 mice. (ns = not significant, $p<0.01$ **).
I) Quantification of relative total cJun levels in the nucleus of retinal ganglion cells in mice treated with vehicle (Veh.) or DLK inhibitor GNE-3511 (DLKi) contralateral (con) and ipsilateral (ipsi) 1 day after optic nerve crush. N=3 mice. (ns = not significant, $p<0.001$ ****).
J) Quantification of relative nuclear p-ATF2 (T71) levels in the nucleus of retinal ganglion cells in mice treated with vehicle (Veh.) or DLK inhibitor GNE-3511 (DLKi) contralateral (con) and ipsilateral (ipsi) 1 day after optic nerve crush. N=3 mice. (ns = not significant, $p<0.01$ **).
K) Quantification of the relative viability of Control, JUN and ATF2 gRNA cortical i^3Neurons Untreated (UT) and transduced with EGFP, ATF2 and ATF2 T69A T71A (ATF2 AA) after treatment for 48 hours with 5 nM vincristine. N=3 independent differentiations. Two-way ANOVA, Bonferroni correction (ns = not significant, $p<0.05$ *, $p<0.01$ **, $p<0.001$ ****).

Figure 5:

A) Representative images of Control, JUN gRNA and ATF2 gRNA cortical i^3Neurons 24 hours after 5nM vincristine treatment. Immunostaining for total cJun (green), DAPI (blue). (Scale bar = 20 µm).
B) Quantification of relative nuclear p-cJun (S63) levels in Control, JUN gRNA and ATF2 gRNA cortical i^3Neurons 24 hours after 5nM vincristine treatment. Results normalized to control gRNA UT. Results are represented as mean ± SEM. N=3 independent differentiations. One-way ANOVA, Bonferroni correction. (ns = not significant, $p<0.005$ ***, $p<0.001$ ****).
C) Quantification of relative nuclear total cJun levels in Control, JUN gRNA and ATF2 gRNA cortical i^3Neurons 24 hours after 5nM vincristine treatment. Results normalized to control gRNA UT. Results are represented as mean ± SEM. N=3 independent differentiations. One-way ANOVA, Bonferroni correction. (ns = not significant, $p<0.01$ **, $p<0.001$ ****).
D) MA plots showing the transcriptional changes in Control, JUN and ATF2 gRNA cortical i^3Neurons 16 hours after 5nM vincristine treatment. Genes that are significantly differentially expressed are labelled in red.
E) Venn diagram showing the common genes regulated by DLK and LZK after vincristine treatment.

Figure 6:

Supplementary Figure 1:

A) Schematic representation of DLK (MAP3K12) knockout (KO) generation strategy. WT i^3 iPSCs were transfected with two gRNAs targeting *DLK* exons 3-5. Primers used for knockout validation flanking *DLK* exons 3-5 are shown in red.
B) Schematic representation of LZK (MAP3K13) knockout (KO) generation strategy. WT i^3 iPSCs were transfected with two gRNAs targeting *DLK* exon 8. Primers used for knockout validation flanking *LZK* exon 8 are shown in red.
C) PCR of WT DLK, LZK and double DLK/LZK KOs using DLK KO primers and LZK KO primers in cortical neuron iPSCs.
D) PCR of WT DLK, LZK and double DLK/LZK KOs using DLK KO primers and LZK KO primers in sensory neuron iPSCs.

Supplementary Figure 2:

A) Schematic representation of the addition of the transcription inhibitor actinomycin D (ActD) 2, 4, 8, and 24 hours after treatment with vincristine.
B) Quantification of the relative viability of cortical i^3Neurons after 48 hours of 5 nM vincristine and ActD at different time points after vincristine treatment N=3 independent differentiations. One-way ANOVA, Bonferroni correction (ns = not significant, $p<0.01$ **, $p<0.005$ ***).

C) Dot plot showing top 10 enriched biological process gene ontology analysis categories for genes enriched in cortical i^3Neurons 16 hours after 5nM vincristine treatment.
D) Positive regulation of apoptosis gene ontology analysis -Log10 false discovery rate (FDR) comparison of genes enriched after vincristine treatment in WT, DLK, LZK and double DLK/LZK KO cortical i^3Neurons.
E) Response to ER stress gene ontology analysis -Log10 false discovery rate (FDR) comparison of genes enriched after vincristine treatment in WT, DLK, LZK and double DLK/LZK KO cortical i^3Neurons.

Supplementary Figure 3:

A) Dot plot showing top 10 enriched biological process gene ontology analysis categories for genes identified to protect neurons from vincristine-induced neurodegeneration in i^3Neurons.
B) Venn diagram showing the common genes regulated in WT i^3neurons after vincristine treatment by RNA seq and genes identified to protect neurons from vincristine-induced neurodegeneration in i^3Neurons.

Supplementary Figure 4:

A) Representative images of WT cortical i^3Neurons UT and 24 hours after 5nM vincristine treatment. Immunostaining for p-P38 (green), p-cJun (S63) (orange) and DAPI (blue). (Scale bar = 20 µm).
B) Quantification of relative nuclear p-P38 (T71) levels UT and after 5 nM vincristine for 24 hours in WT cortical i^3Neurons. Results normalized to WT UT. Results are represented as mean ± SEM. N=3 independent differentiations. Two-way ANOVA, Bonferroni correction. (ns = not significant).
C) Quantification of the relative viability of cortical i^3Neurons after 48 hours of 5 nM vincristine, 5 nM vincristine + 100 nM P38 inhibitor. N=3 independent differentiations. Two-way ANOVA, Bonferroni correction (ns = not significant

Supplementary Figure 5:

A) MA plots showing the transcriptional changes in untreated (UT) ATF2 gRNA neurons compared to control gRNA. Genes that are significantly differentially expressed are labelled in red.
B) MA plots showing the transcriptional changes in untreated (UT) JUN gRNA neurons compared to control gRNA. Genes that are significantly differentially expressed are labelled in red.

References

1 Shen S, Shao Y, Li C. Different types of cell death and their shift in shaping disease. *Cell Death Discov* 2023; **9**: 284.

2 Nihalani D, Merritt S, Holzman LB. Identification of Structural and Functional Domains in Mixed Lineage Kinase Dual Leucine Zipper-bearing Kinase Required for Complex Formation and Stress-activated Protein Kinase Activation*. *J Biol Chem* 2000; **275**: 7273–7279.

3 Saikia JM, Chavez-Martinez CL, Kim ND, Allibhoy S, Kim HJ, Simonyan L *et al.* A Critical Role for DLK and LZK in Axonal Repair in the Mammalian Spinal Cord. *J Neurosci* 2022; **42**: 3716–3732.

4 Welsbie DS, Mitchell KL, Jaskula-Ranga V, Sluch VM, Yang Z, Kim J *et al.* Enhanced Functional Genomic Screening Identifies Novel Mediators of Dual Leucine Zipper Kinase-Dependent Injury Signaling in Neurons. *Neuron* 2017; **94**: 1142-1154.e6.

5 Alexandris AS, Lee Y, Lehar M, Alam Z, McKenney J, Perdomo D *et al.* Traumatic axonal injury in the optic nerve: the selective role of SARM1 in the evolution of distal axonopathy. *J Neurotraum* 2022; **0**. doi:10.1089/neu.2022.0416.

6 Adula KP, Shorey M, Chauhan V, Nassman K, Chen S-F, Rolls MM *et al.* The MAP3Ks DLK and LZK Direct Diverse Responses to Axon Damage in Zebrafish Peripheral Neurons. *J Neurosci* 2022; **42**: 6195–6210.

7 Li Y, Ritchie EM, Steinke CL, Qi C, Chen L, Zheng B *et al.* Activation of MAP3K DLK and LZK in Purkinje cells causes rapid and slow degeneration depending on signaling strength. *eLife* 2021; **10**: e63509.

8 Patel S, Cohen F, Dean BJ, Torre KDL, Deshmukh G, Estrada AA *et al.* Discovery of Dual Leucine Zipper Kinase (DLK, MAP3K12) Inhibitors with Activity in Neurodegeneration Models. *J Med Chem* 2015; **58**: 401–418.

9 Craig RA, Fox BM, Hu C, Lexa KW, Osipov M, Thottumkara AP *et al.* Discovery of Potent and Selective Dual Leucine Zipper Kinase/Leucine Zipper-Bearing Kinase Inhibitors with Neuroprotective Properties in In Vitro and In Vivo Models of Amyotrophic Lateral Sclerosis. *J Med Chem* 2022. doi:10.1021/acs.jmedchem.2c01056.

10 Le K, Soth MJ, Cross JB, Liu G, Ray WJ, Ma J *et al.* Discovery of IACS-52825, a Potent and Selective DLK Inhibitor for Treatment of Chemotherapy-Induced Peripheral Neuropathy. *J Med Chem* 2023. doi:10.1021/acs.jmedchem.3c00788.

11 Patel S, Meilandt WJ, Erickson RI, Chen J, Deshmukh G, Estrada AA *et al.* Selective Inhibitors of Dual Leucine Zipper Kinase (DLK, MAP3K12) with Activity in a Model of Alzheimer's Disease. *J Med Chem* 2017; **60**: 8083–8102.

12 Katz JS, Rothstein JD, Cudkowicz ME, Genge A, Oskarsson B, Hains AB *et al.* A Phase 1 study of GDC-0134, a dual leucine zipper kinase inhibitor, in ALS. *Ann Clin Transl Neur* 2022; **9**: 50–66.

13 Adib EA, Smithson LJ, Collins CA. An axonal stress response pathway: degenerative and regenerative signaling by DLK. *Curr Opin Neurobiol* 2018; **53**: 110–119.

14 Behrens A, Sibilia M, Wagner EF. Amino-terminal phosphorylation of c-Jun regulates stress-induced apoptosis and cellular proliferation. *Nat Genet* 1999; **21**: 326–329.

15 Keramaris E, Vanderluit JL, Bahadori M, Mousavi K, Davis RJ, Flavell R *et al.* c-Jun N-terminal Kinase 3 Deficiency Protects Neurons from Axotomy-induced Death in Vivo through Mechanisms Independent of c-Jun Phosphorylation*. *J Biol Chem* 2005; **280**: 1132–1141.

16 Ruff CA, Staak N, Patodia S, Kaswich M, Rocha-Ferreira E, Costa CD *et al.* Neuronal c-Jun is required for successful axonal regeneration, but the effects of phosphorylation of its N-terminus are moderate. *J Neurochem* 2012; **121**: 607–618.

17 Reddy CE, Albanito L, Marco PD, Aiello D, Maggiolini M, Napoli A *et al.* Multisite phosphorylation of c-Jun at threonine 91/93/95 triggers the onset of c-Jun pro-apoptotic activity in cerebellar granule neurons. *Cell Death Dis* 2013; **4**: e852–e852.

18 Besirli CG, Wagner EF, Johnson EM. The limited role of NH2-terminal c-Jun phosphorylation in neuronal apoptosis. *The J Cell Biology* 2005; **170**: 401–411.

19 Wu Z, Nicoll M, Ingham RJ. AP-1 family transcription factors: a diverse family of proteins that regulate varied cellular activities in classical hodgkin lymphoma and ALK+ ALCL. *Exp Hematol Oncol* 2021; **10**: 4.

20 Shaulian E, Karin M. AP-1 in cell proliferation and survival. *Oncogene* 2001; **20**: 2390–2400.

21 Tian F, Cheng Y, Zhou S, Wang Q, Monavarfeshani A, Gao K *et al.* Core transcription programs controlling injury-induced neurodegeneration of retinal ganglion cells. *Neuron* 2022; **110**: 2607-2624.e8.

22 Renthal W, Tochitsky I, Yang L, Cheng Y-C, Li E, Kawaguchi R *et al.* Transcriptional Reprogramming of Distinct Peripheral Sensory Neuron Subtypes after Axonal Injury. *Neuron* 2020. doi:10.1016/j.neuron.2020.07.026.

23 Somasundaram P, Farley MM, Rudy MA, Stefanoff DG, Shah M, Goli P *et al.* Coordinated stimulation of axon regenerative and neurodegenerative transcriptional programs by Atf4 following optic nerve injury. 2023. doi:10.7554/elife.87528.

24 Nguyen MQ, Le Pichon CE, Ryba N. Stereotyped transcriptomic transformation of somatosensory neurons in response to injury. *Elife* 2019; **8**: e49679.

25 Kirsch K, Zeke A, Tőke O, Sok P, Sethi A, Sebő A *et al.* Co-regulation of the transcription controlling ATF2 phosphoswitch by JNK and p38. *Nat Commun* 2020; **11**: 5769.

26 Liu H, Deng X, Shyu YJ, Li JJ, Taparowsky EJ, Hu C. Mutual regulation of c-Jun and ATF2 by transcriptional activation and subcellular localization. *EMBO J* 2006; **25**: 1058–1069.

27 Ackermann J, Ashton G, Lyons S, James D, Hornung J-P, Jones N *et al.* Loss of ATF2 Function Leads to Cranial Motoneuron Degeneration during Embryonic Mouse Development. *PLoS ONE* 2011; **6**: e19090.

28 Saha P, Guha S, Biswas SC. P38K and JNK pathways are induced by amyloid-β in astrocyte: Implication of MAPK pathways in astrogliosis in Alzheimer's disease. *Mol Cell Neurosci* 2020; **108**: 103551.

29 Yamada T, Yoshiyama Y, Kawaguchi N. Expression of activating transcription factor-2 (ATF-2), one of the cyclic AMP response element (CRE) binding proteins, in Alzheimer disease and non-neurological brain tissues. *Brain Res* 1997; **749**: 329–334.

30 Huang Q, Du X, He X, Yu Q, Hu K, Breitwieser W *et al.* JNK-mediated activation of ATF2 contributes to dopaminergic neurodegeneration in the MPTP mouse model of Parkinson's disease. *Exp Neurol* 2016; **277**: 296–304.

31 Wang C, Ward ME, Chen R, Liu K, Tracy TE, Chen X *et al.* Scalable Production of iPSC-Derived Human Neurons to Identify Tau-Lowering Compounds by High-Content Screening. *Stem Cell Rep* 2017; **9**: 1221–1233.

32 Nickolls AR, Lee MM, Espinoza DF, Szczot M, Lam RM, Wang Q *et al.* Transcriptional Programming of Human Mechanosensory Neuron Subtypes from Pluripotent Stem Cells. *Cell Reports* 2020; **30**: 932-946.e7.

33 Duffy EE, Finander B, Choi G, Carter AC, Pritisanac I, Alam A *et al.* Developmental dynamics of RNA translation in the human brain. *Nat Neurosci* 2022; **25**: 1353–1365.

34 Geisler S, Doan RA, Cheng GC, Cetinkaya-Fisgin A, Huang SX, Höke A *et al.* Vincristine and bortezomib use distinct upstream mechanisms to activate a common SARM1-dependent axon degeneration program. *Jci Insight* 2019; **4**: e129920.

35 Gomez-Deza J, Slavutsky AL, Nebiyou M, Le Pichon CE. Local production of reactive oxygen species drives vincristine-induced axon degeneration. *Biorxiv* 2022; : 2022.07.30.501173.

36 Lu C, Zhu F, Cho Y-Y, Tang F, Zykova T, Ma W *et al.* Cell Apoptosis: Requirement of H2AX in DNA Ladder Formation, but Not for the Activation of Caspase-3. *Mol Cell* 2006; **23**: 121–132.

37 Holland SM, Collura KM, Ketschek A, Noma K, Ferguson TA, Jin Y *et al.* Palmitoylation controls DLK localization, interactions and activity to ensure effective axonal injury signaling. *Proc National Acad Sci* 2016; **113**: 763–768.

38 Larhammar M, Huntwork-Rodriguez S, Jiang Z, Solanoy H, Ghosh AS, Wang B *et al.* Dual leucine zipper kinase-dependent PERK activation contributes to neuronal degeneration following insult. *Elife* 2017; **6**: e20725.

39 Ghosh AS, Wang B, Pozniak CD, Chen M, Watts RJ, Lewcock JW. DLK induces developmental neuronal degeneration via selective regulation of proapoptotic JNK activity. *J Cell Biology* 2011; **194**: 751–764.

40 Alerasool N, Segal D, Lee H, Taipale M. An efficient KRAB domain for CRISPRi applications in human cells. *Nat Methods* 2020; **17**: 1093–1096.

41 Watson G, Ronai Z, Lau E. ATF2, a paradigm of the multifaceted regulation of transcription factors in biology and disease. *Pharmacol Res* 2017; **119**: 347–357.

42 Watkins TA, Wang B, Huntwork-Rodriguez S, Yang J, Jiang Z, Eastham-Anderson J *et al.* DLK initiates a transcriptional program that couples apoptotic and regenerative responses to axonal injury. *Proc National Acad Sci* 2013; **110**: 4039–4044.

43 Le Pichon CE, Meilandt WJ, Dominguez S, Solanoy H, Lin H, Ngu H *et al.* Loss of dual leucine zipper kinase signaling is protective in animal models of neurodegenerative disease. *Sci Transl Med* 2017; **9**: eaag0394.

44 Wlaschin JJ, Donahue C, Gluski J, Osborne JF, Ramos LM, Silberberg H *et al.* Promoting regeneration while blocking cell death preserves motor neuron function in a model of ALS. *Brain* 2022; **146**: 2016–2028.

45 Fernandes KA, Harder JM, John SW, Shrager P, Libby RT. DLK-dependent signaling is important for somal but not axonal degeneration of retinal ganglion cells following axonal injury. *Neurobiol Dis* 2014; **69**: 108–116.

46 Valakh V, Frey E, Babetto E, Walker LJ, DiAntonio A. Cytoskeletal disruption activates the DLK/JNK pathway, which promotes axonal regeneration and mimics a preconditioning injury. *Neurobiol Dis* 2015; **77**: 13–25.

47 Bates D, Eastman A. Microtubule destabilising agents: far more than just antimitotic anticancer drugs. *Brit J Clin Pharmaco* 2017; **83**: 255–268.

48 Gasic I, Boswell SA, Mitchison TJ. Tubulin mRNA stability is sensitive to change in microtubule dynamics caused by multiple physiological and toxic cues. *Plos Biol* 2019; **17**: e3000225.

49 Höpfler M, Absmeier E, Peak-Chew S-Y, Vartholomaiou E, Passmore LA, Gasic I *et al.* Mechanism of ribosome-associated mRNA degradation during tubulin autoregulation. *Mol Cell* 2023; **83**: 2290-2302.e13.

50 Lin Z, Gasic I, Chandrasekaran V, Peters N, Shao S, Mitchison TJ *et al.* TTC5 mediates autoregulation of tubulin via mRNA degradation. *Science* 2020; **367**: 100–104.

51 Ries V, Silva RM, Oo TF, Cheng H, Rzhetskaya M, Kholodilov N *et al.* JNK2 and JNK3 combined are essential for apoptosis in dopamine neurons of the substantia nigra, but are not required for axon degeneration. *J Neurochem* 2008; **107**: 1578–1588.

52 Guo X, Zhou J, Starr C, Mohns EJ, Li Y, Chen EP *et al.* Preservation of vision after CaMKII-mediated protection of retinal ganglion cells. *Cell* 2021; **184**: 4299-4314.e12.

53 Kirwan P, Jura M, Merkle FT. Generation and Characterization of Functional Human Hypothalamic Neurons. *Curr Protoc Neurosci* 2017; **81**: 3.33.1-3.33.24.

54 Bodapati S, Daley TP, Lin X, Zou J, Qi LS. A benchmark of algorithms for the analysis of pooled CRISPR screens. *Genome Biol* 2020; **21**: 62.

55 Dobin A, Davis CA, Schlesinger F, Drenkow J, Zaleski C, Jha S *et al.* STAR: ultrafast universal RNA-seq aligner. *Bioinformatics* 2013; **29**: 15–21.

56 Liao Y, Smyth GK, Shi W. featureCounts: an efficient general purpose program for assigning sequence reads to genomic features. *Bioinformatics* 2014; **30**: 923–930.

57 Stephens M. False discovery rates: a new deal. *Biostatistics* 2016; **18**: kxw041.

58 Benjamini Y, Hochberg Y. Controlling the False Discovery Rate: A Practical and Powerful Approach to Multiple Testing. *J R Stat Soc: Ser B (Methodol)* 1995; **57**: 289–300.

Figure 1

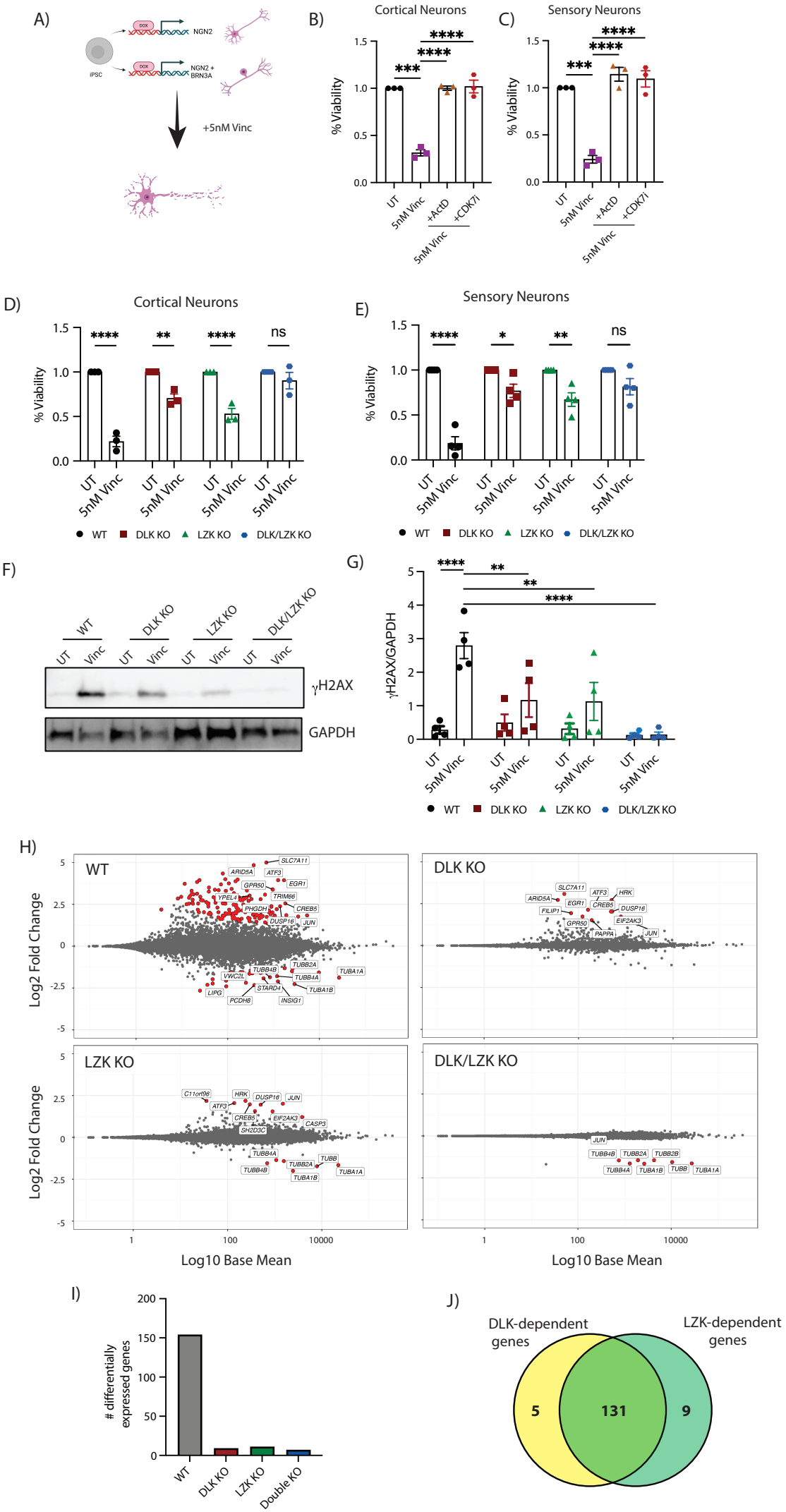
A)
dox
NGN2
iPSC
dox
NGN2 + BRN3A
+5nM Vinc
B)
Cortical Neurons
% Viability
UT
5nM Vinc
+ActD
+CDK7i
5nM Vinc
C)
Sensory Neurons
D)
Cortical Neurons
E)
Sensory Neurons
WT
DLK KO
LZK KO
DLK/LZK KO
F)
WT
DLK KO
LZK KO
DLK/LZK KO
UT
Vinc
γH2AX
GAPDH
G)
γH2AX/GAPDH
H)
WT
DLK KO
LZK KO
DLK/LZK KO
Log2 Fold Change
Log10 Base Mean
I)
differentially expressed genes
WT
DLK KO
LZK KO
Double KO
J)
DLK-dependent genes
LZK-dependent genes
5
131
9

Figure 2

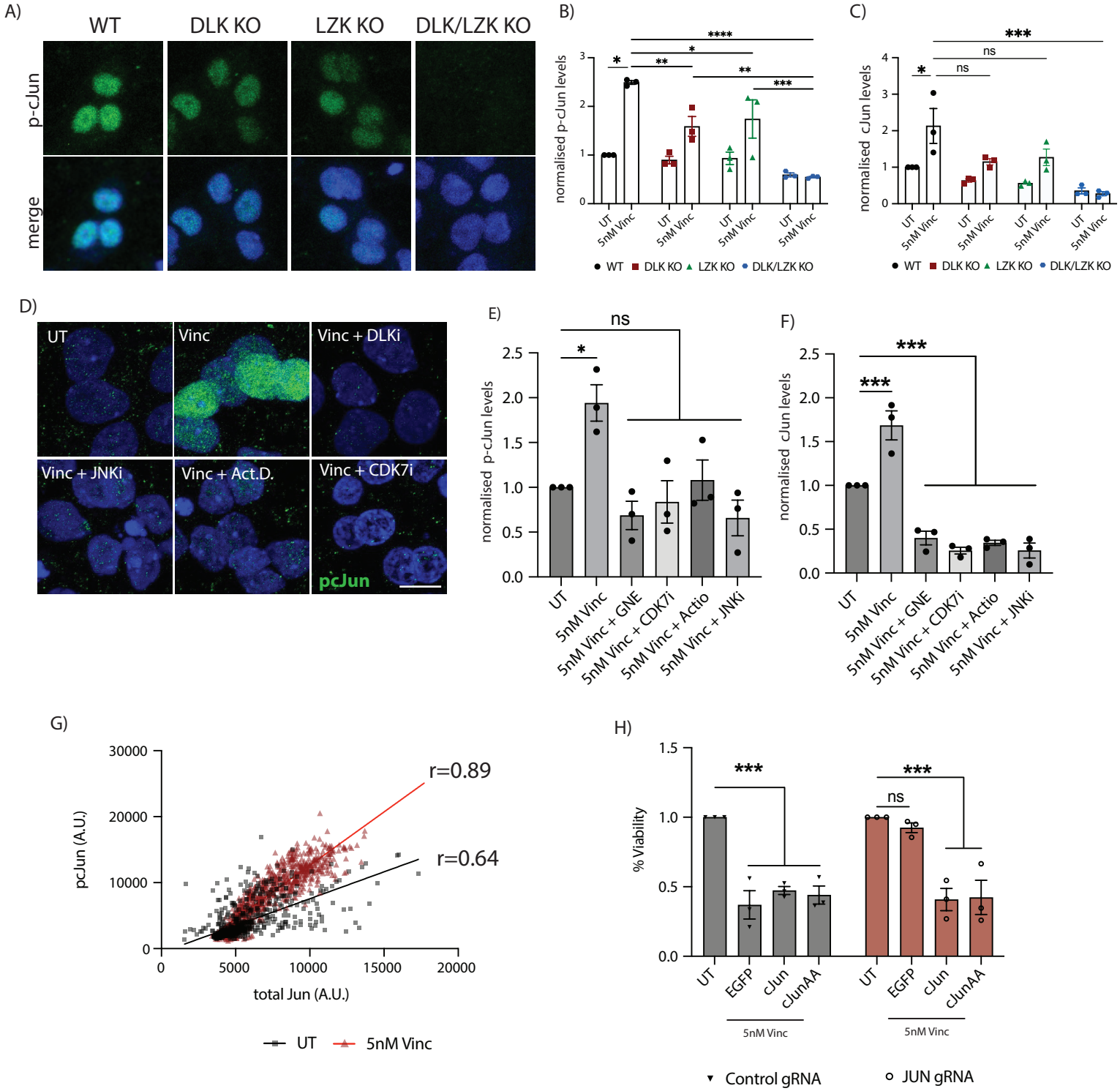
A)
WT
DLK KO
LZK KO
DLK/LZK KO
p-cJun
merge
B)
normalised p-cJun levels
UT
5nM Vinc
WT
DLK KO
LZK KO
DLK/LZK KO
C)
normalised cJun levels
D)
UT
Vinc
Vinc + DLKi
Vinc + JNKi
Vinc + Act.D.
Vinc + CDK7i
pcJun
E)
normalised p-cJun levels
ns
5nM Vinc + GNE
5nM Vinc + CDK7i
5nM Vinc + Actio
5nM Vinc + JNKi
F)
normalised cJun levels
G)
pcJun (A.U.)
total Jun (A.U.)
r=0.89
r=0.64
UT
5nM Vinc
H)
% Viability
EGFP
cJun
cJunAA
5nM Vinc
Control gRNA
JUN gRNA

Figure 3

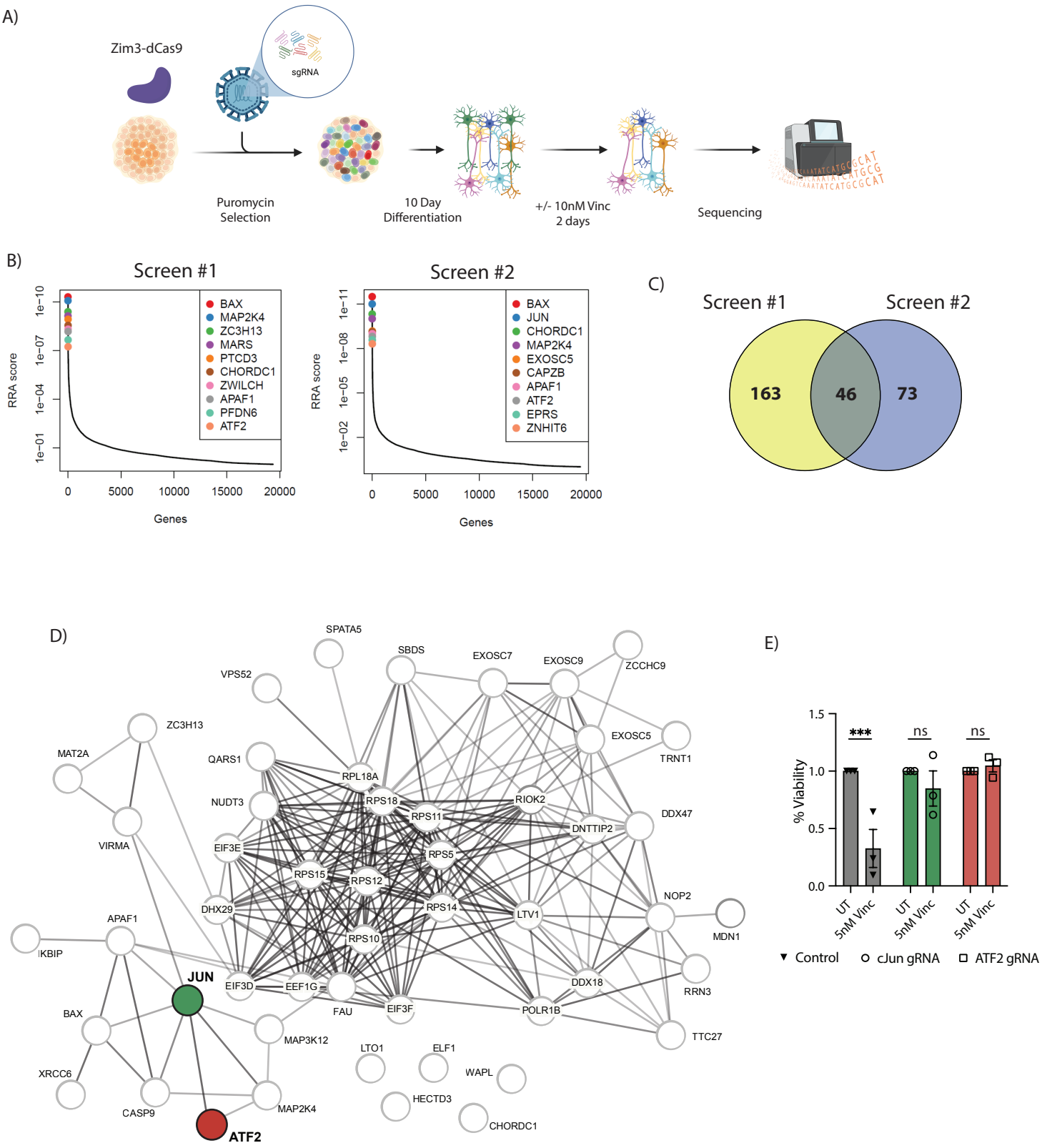
A)
Zim3-dCas9
sgRNA
Puromycin Selection
10 Day Differentiation
+/- 10nM Vinc 2 days
Sequencing
B)
Screen #1
Screen #2
RRA score
Genes
BAX
MAP2K4
ZC3H13
MARS
PTCD3
CHORDC1
ZWILCH
APAF1
PFDN6
ATF2
JUN
CHORDC1
MAP2K4
EXOSC5
CAPZB
APAF1
ATF2
EPRS
ZNHIT6
C)
Screen #1
Screen #2
163
46
73
D)
SPATA5
SBDS
EXOSC7
EXOSC9
ZCCHC9
VPS52
ZC3H13
MAT2A
QARS1
EXOSC5
TRNT1
RPL18A
NUDT3
RPS18
RIOK2
RPS11
DDX47
DNTTIP2
VIRMA
EIF3E
RPS5
RPS15
RPS12
NOP2
DHX29
RPS14
LTV1
APAF1
MDN1
IKBIP
RPS10
JUN
EIF3D
EEF1G
DDX18
RRN3
FAU
EIF3F
POLR1B
BAX
MAP3K12
TTC27
LTO1
ELF1
XRCC6
WAPL
HECTD3
CASP9
MAP2K4
CHORDC1
ATF2
E)
% Viability
***
ns
ns
UT
5nM Vinc
Control
cJun gRNA
ATF2 gRNA

Figure 4

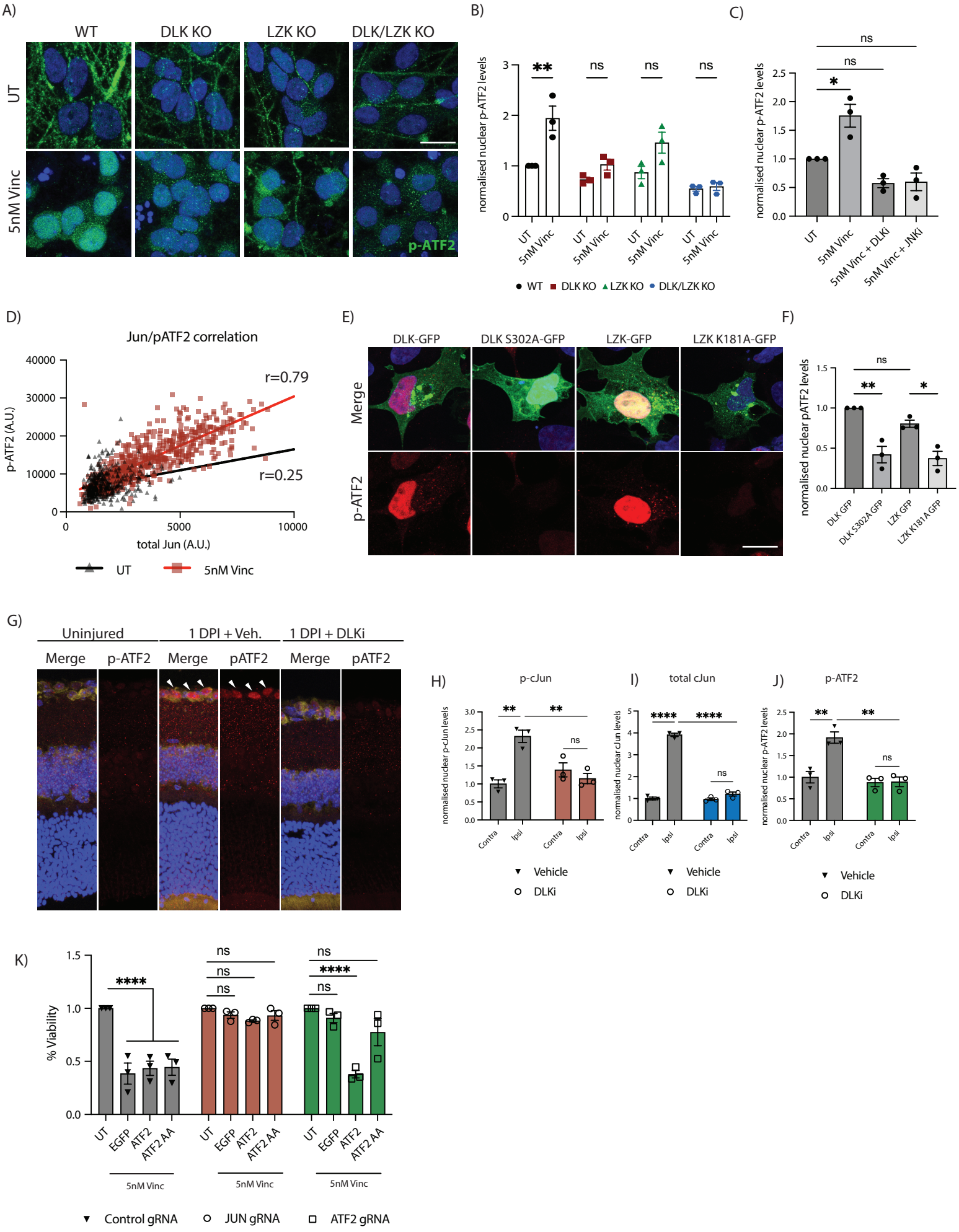
A)
WT
DLK KO
LZK KO
DLK/LZK KO
UT
5nM Vinc
p-ATF2
B)
normalised nuclear p-ATF2 levels
**
ns
ns
ns
UT
5nM Vinc
WT
DLK KO
LZK KO
DLK/LZK KO
C)
ns
ns
*
normalised nuclear p-ATF2 levels
UT
5nM Vinc
5nM Vinc + DLKi
5nM Vinc + JNKi
D)
Jun/pATF2 correlation
r=0.79
r=0.25
p-ATF2 (A.U.)
total Jun (A.U.)
UT
5nM Vinc
E)
DLK-GFP
DLK S302A-GFP
LZK-GFP
LZK K181A-GFP
Merge
p-ATF2
F)
ns
**
*
normalised nuclear pATF2 levels
DLK GFP
DLK S302A GFP
LZK GFP
LZK K181A GFP
G)
Uninjured
1 DPI + Veh.
1 DPI + DLKi
Merge
p-ATF2
Merge
pATF2
Merge
pATF2
H)
p-cJun
normalised nuclear p-cJun levels
**
**
ns
Contra
Ipsi
Vehicle
DLKi
I)
total cJun
normalised nuclear cJun levels
****
****
ns
Contra
Ipsi
Vehicle
DLKi
J)
p-ATF2
normalised nuclear p-ATF2 levels
**
**
ns
Contra
Ipsi
Vehicle
DLKi
K)
% Viability
****
ns
ns
ns
ns
****
ns
UT
EGFP
ATF2
ATF2 AA
5nM Vinc
Control gRNA
JUN gRNA
ATF2 gRNA

Figure 5

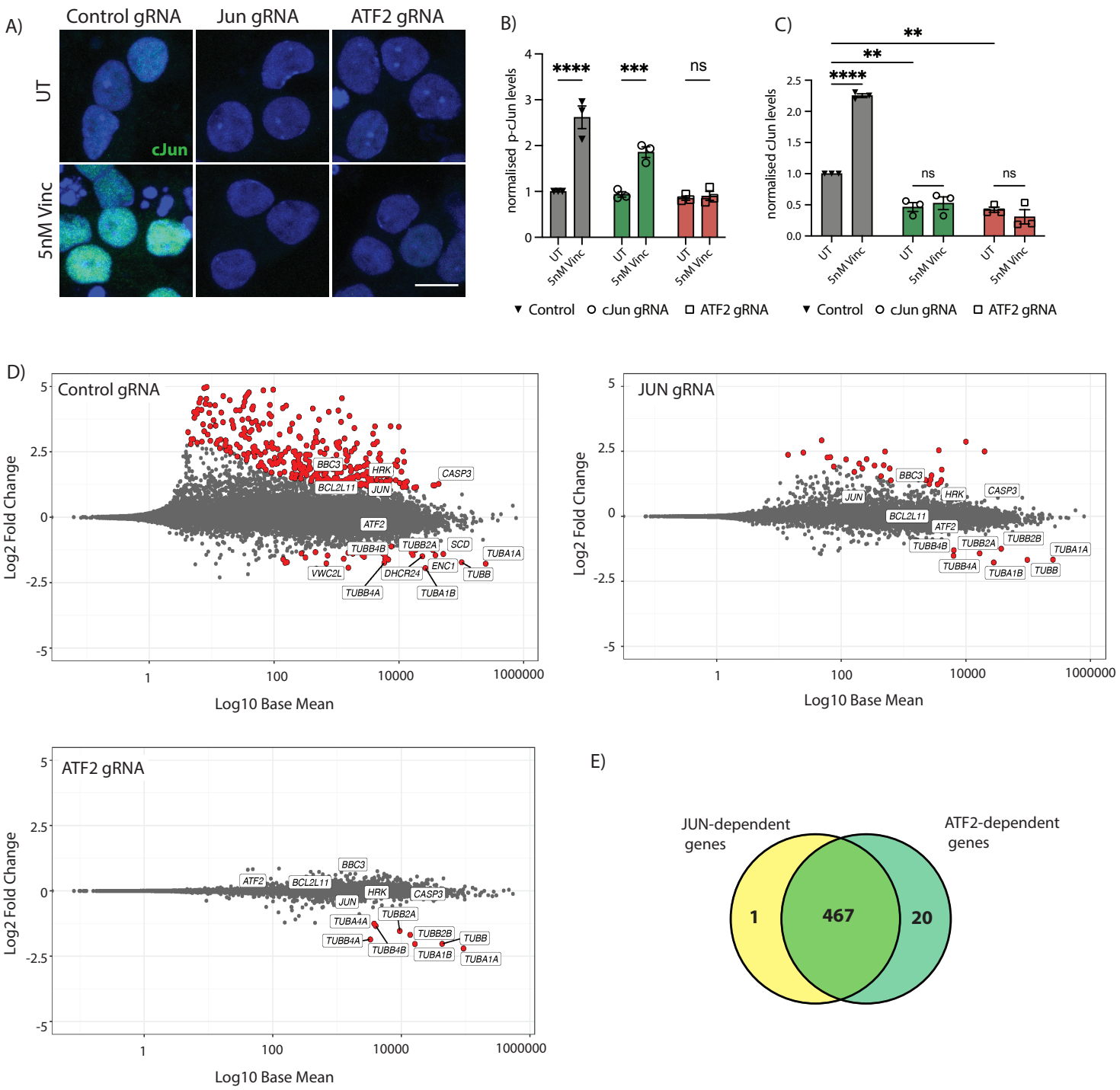
A)
Control gRNA
Jun gRNA
ATF2 gRNA
UT
5nM Vinc
cJun
B)
normalised p-cJun levels
****
***
ns
UT
5nM Vinc
▼ Control ○ cJun gRNA □ ATF2 gRNA
C)
normalised cJun levels
**
****
ns
▼ Control ○ cJun gRNA □ ATF2 gRNA
D)
Control gRNA
JUN gRNA
ATF2 gRNA
Log2 Fold Change
Log10 Base Mean
BBC3
HRK
CASP3
BCL2L11
JUN
ATF2
TUBB4B
TUBB2A
SCD
TUBA1A
VWC2L
DHCR24
ENC1
TUBB
TUBB4A
TUBA1B
TUBB2B
E)
JUN-dependent genes
ATF2-dependent genes
1
467
20
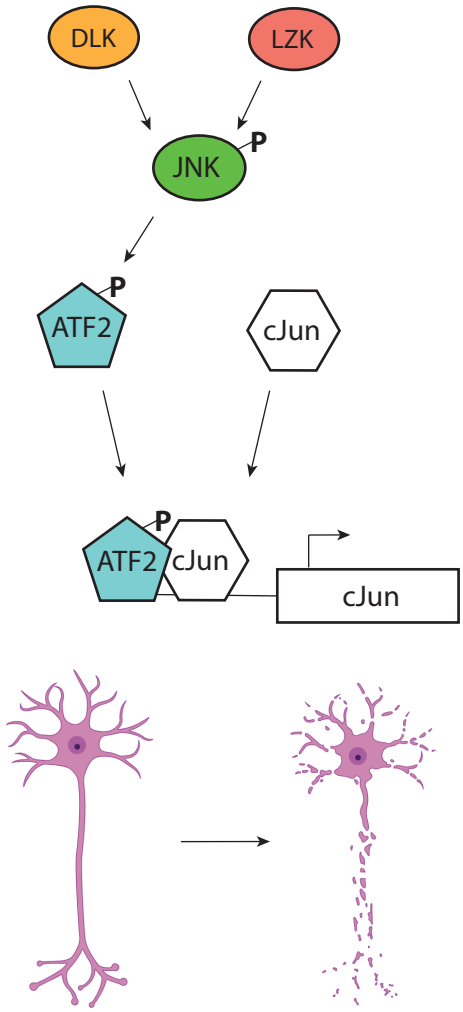
Figure 6